Iridium Clusters in NaX Zeolite Cages: Synthesis, Reactivity, and Characterization by Infrared and Extended X-ray Absorption Fine Structure Spectroscopies

S. Kawi and B. C. Gates*

Center for Catalytic Science and Technology, Department of Chemical Engineering, University of Delaware, Newark, Delaware 19716

Received: January 16, 1995; In Final Form: March 20, 1995[⊗]

$[Ir(CO)_2(acac)]$ in the pores of NaX zeolite was treated in CO and converted into iridium carbonyl clusters, which are suggested on the basis of infrared spectra and comparisons with solution chemistry to be $[HIr_4(CO)_{11}]^-$, which was subsequently converted into clusters that are suggested to be $[Ir_6(CO)_{15}]^{2-}$. The former clusters in the NaX zeolite were decarbonylated by treatment in He followed by H_2 at 573 K and characterized by extended X-ray absorption fine structure spectroscopy. The Ir−Ir first-shell coordination number (3.0) indicates that the clusters were predominantly Ir_4 tetrahedra. The clusters postulated to be $[Ir_6(CO)_{15}]^{2-}$ were reversibly fragmented and reformed in the cages.

Introduction

Nanostructures dispersed in the molecular-scale cages of zeolites range from metals,[1] which are potential shape-selective supported catalysts, to metal oxides[2,3] and metal sulfides,[4,5] which are semiconductors that may offer novel electronic and optical properties. Understanding of the chemistry of these structures is difficult because most of these materials are structurally nonuniform.

Metal carbonyl clusters have been used as precursors in attempts to prepare supported catalysts with uniform and nearly molecular structures.[6] However, most of the attempts to form uniform decarbonylated clusters in zeolite cages have been unsuccessful because decarbonylation of the clusters, which are formed by "ship-in-a-bottle" syntheses, typically leads to fragmentation and/or aggregation of metal, yielding mixtures of clusters not only inside the cages but also outside the zeolite crystallites. However, decarbonylation of robust metal carbonyl clusters has been shown by extended X-ray absorption fine structure (EXAFS) spectroscopy to give nearly uniform Ir_4 on MgO,[7,8] Pt_{15} on MgO,[9] and Os_{10} on MgO,[10] Ir_4 in NaY zeolite,[11,12] and Ir_6 in NaY zeolite.[13,14]

Here we report the synthesis and chemistry of iridium carbonyl clusters formed from $[Ir(CO)_2(acac)]$ in NaX zeolite cages.[15] NaX zeolite was chosen because it is moderately basic, and the synthesis of iridium carbonyl cluster anions occurs in basic solutions.[16−20] $[Ir(CO)_2(acac)]$ was chosen as the organometallic precursor because it offers the following advantages: (1) it has no chloride or other components that are expected to be catalyst poisons; (2) it is small enough to diffuse readily into the zeolite channels; and (3) it is converted into iridium carbonyl clusters on metal oxide surfaces in relatively well understood chemistry.[21,22]

Experimental Methods

Materials and Sample Preparation. Synthesis of the zeolite-supported iridium carbonyls was performed with samples in a Braun MB-150M glovebox purged with N_2 that recirculated through O_2- and moisture-scavenging traps or on a Schlenk vacuum line that was purged with N_2 (99.999%). The drybox was equipped with O_2 and moisture detectors that consistently indicated concentrations of these contaminants <1 ppm. NaX zeolite powder was supplied by Union Carbide (Linde type 13X, silica/alumina molar ratio about 2.5). Prior to preparation of the zeolite-supported samples, the zeolite was evacuated at 10^{-3} Torr at room temperature for 2 h, but it was not rigorously dried. $[Ir(CO)_2(acac)]$ (Strem) was used without purification. Reagent grade mixed hexanes were purged with N_2 for several hours before use as a solvent. He and H_2 (Matheson, 99.999%) were purified by passage through traps containing particles of Cu_2O and particles of activated zeolite 4A to remove traces of O_2 and moisture, respectively. CO (Matheson, UHP grade) was purified by passage through a trap containing particles of activated alumina heated to a temperature exceeding 523 K to remove traces of metal carbonyls from the high-pressure gas cylinder and through a trap containing particles of activated zeolite 4A to remove moisture.

In the preparation of the zeolite-supported iridium-containing samples, $[Ir(CO)_2(acac)]$ (30 mg/g of NaX to make a sample containing 0.8 wt % Ir) was dissolved in hexanes and brought in contact with the preevacuated NaX zeolite. The light brown NaX powder became dark brownish green, and the initially greenish-black solution became clearer after stirring for several hours. After 2 days of stirring, the uptake of $[Ir(CO)_2(acac)]$ was complete; the hexane solution was clear, and no $[Ir(CO)_2(acac)]$ was detected in the solution by infrared spectroscopy. The metal-containing zeolite was separated by filtration, washed thoroughly with hexane, and dried under vacuum at room temperature for 12 h. The samples were stored in the drybox.

Infrared Spectroscopy. Transmission infrared spectra of the zeolite samples were collected with a Nicolet 7199 FTIR spectrometer with a resolution of 4 cm^{-1}. Samples were pressed into semitransparent wafers in the drybox and mounted in the infrared cell. The experiments were performed with the samples in controlled atmospheres; purified He, N_2, CO, or H_2 could be delivered to the cell, which was part of a flow system. A typical gas flow rate was 20−30 mL (NTP)/min. Samples were scanned 32 or more times and the data averaged.

Extended X-ray Absorption Fine Structure (EXAFS) Spectroscopy. The EXAFS experiments were performed on X-ray beamline X-11A at the National Synchrotron Light Source at Brookhaven National Laboratory, Upton, Long Island, NY. The ring energy was 2.5 GeV, and the ring current 80−220

* To whom correspondence should be addressed at Department of Chemical Engineering and Materials Science, University of California, Davis, CA 95616.

[⊗] Abstract published in *Advance ACS Abstracts,* May 1, 1995.

0022-3654/95/2099-8824$09.00/0

TABLE 1: Crystallographic Data Characterizing the Reference Compounds and Fourier Transform Ranges Used in the EXAFS Analysis[a]

	crystallographic data			Fourier transform		
sample	shell	N	R, Å	Δk, Å^{-1}	Δr, Å	n
Pt foil	Pt−Pt[b]	12	2.77	1.9−19.8	1.9−3.0	3
$Na_2Pt(OH)_6$	Pt−O[c]	6	2.05	1.4−17.7	0.5−2.0	3
$[Ir_4(CO)_{12}]$	Ir−C[d]	3	1.87	2.8−16.5	1.1−2.0	3

[a] Notation: N, coordination number for absorber−backscatterer pair; R, radial distance from crystal structure data; Δk limits used for forward Fourier transformation (k is the wave vector); Δr, limits used for shell isolation (r is distance); n, power of k used for Fourier transformation. [b] Crystal structure data from ref 23. [c] Crystal structure data from ref 24. [d] Crystal structure data from ref 26; after subtraction of the Ir−Ir contribution: $N = 6$, $R = 2.69$ Å, $\Delta\sigma^2$ (Debye−Waller factor; difference with respect to reference compounds) = −0.001 Å^2, and ΔE_0 (inner potential correction of the edge position) = 2.5 eV.

mA. The spectra were recorded with the sample in a cell that allowed treatment in flowing gases prior to the measurements. The powder samples were pressed into wafers with a C-clamp inside a glovebag purged with N_2 boiloff gas from a liquid nitrogen cylinder. The amount of sample in a wafer (approximately 150 mg) was calculated to give an absorbance of 2.5 at the Ir L_{III} absorption edge. After the sample had been pressed, it was unloaded from the die and loaded into the EXAFS cell. The cell was then sealed under a positive pressure of N_2, removed from the glovebag, aligned in the X-ray beam, and cooled with liquid nitrogen. The EXAFS data, recorded in the transmission mode, were collected with a Si(111) double-crystal monochromator that was detuned by 30% to minimize the effects of higher harmonics in the X-ray beam. Each sample was scanned three times at energies near the Ir L_{III} absorption edge (11215 eV).

The sample was prepared by adsorption of $[Ir(CO)_2(acac)]$ in NaX zeolite followed by treatment in a glass reactor at the University of Delaware with flowing CO at 348 K and 1 bar for 8 h. The sample was removed from the reactor inside the drybox. It was stored in three layers of glass vials that were sealed with parafilm. The sample was transported to the synchrotron, where it was pressed and loaded into the EXAFS cell. The sample in the EXAFS cell was treated in flowing He [60 mL (NTP)/min] at 573 K for 2 h and then cooled to room temperature in flowing He. It was then treated in flowing H_2 [60 mL (NTP)/min] at 573 K for 2 h and cooled to room temperature in flowing H_2. The cell was then sealed under a positive pressure of H_2 and cooled to approximately liquid nitrogen temperature before data collection.

EXAFS Reference Data. The EXAFS data were analyzed with experimentally determined reference files obtained from EXAFS data for materials of known structure. The Ir−Ir and Ir−$O_{support}$ interactions were analyzed with phase shifts and backscattering amplitudes obtained from EXAFS data for Pt foil[23] and $Na_2Pt(OH)_6$,[24] respectively. The transferability of the phase shift and backscattering amplitudes for Pt and Ir is justified by experimental results.[25] The Ir−C interaction was analyzed with the phase shift and backscattering amplitude obtained from EXAFS data for crystalline $[Ir_4(CO)_{12}]$[26] that was mixed with SiO_2. Details of the preparation of the reference files are given elsewhere,[27] and the parameters used to extract these files from the EXAFS data are summarized in Table 1.

Results

Reactivity of $[Ir(CO)_2(acac)]$ in NaX Zeolite in the Presence of CO at 1 bar. The infrared spectrum of the freshly prepared $[Ir(CO)_2(acac)]$-containing zeolite (a brownish-yellow

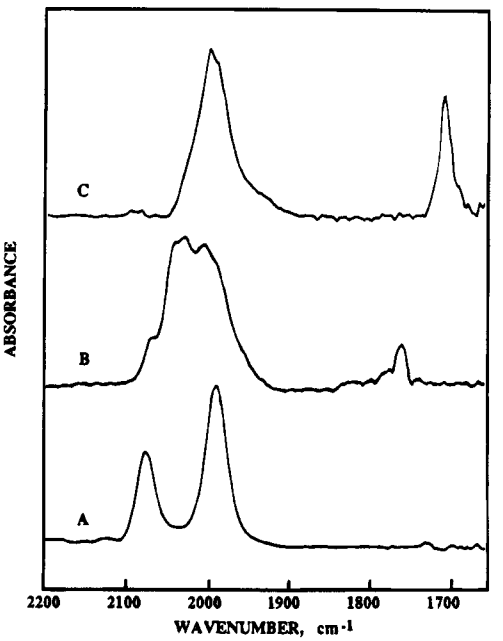

Figure 1. Infrared spectra taken during treatment of the initially prepared sample made from $[Ir(CO)_2(acac)]$ and NaX zeolite: (A) $[Ir(CO)_2(acac)]$ adsorbed in NaX zeolite; (B) after treatment in CO at 348 K for 8 h; (C) after treatment in CO at 448 K for 2 h.

TABLE 2: Infrared Spectra in the Carbonyl Stretching Region Characterizing NaX-Supported Iridium Carbonyl Species and Related Molecular Iridium Clusters

sample	ν_{CO}, cm^{-1}	ref
$[Ir(CO)_2(acac)]$ in NaX (1A)	2082 s, 1984 s	this work
1A, then CO at 348 K, 8 h (1B)	2072 w, 2044 sh, 2035 s, 2011 m, 2000 sh, 1765 mw	this work
1B, then CO at 448 K, 2 h	2001 s, 1993 s, 1710 m	this work
$[NEt_4][HIr_4(CO)_{11}]$ in THF	2067 w, 2030 sh, 2017 vs, 1986 m, 1978 m, 1832 m	*a*
$Na[HIr_4(CO)_{11}]$ in diethyl ether	2072 w, 2039 s, 2020 vs, 1990 m, 1984 m, 1830 w, 1730 m	*a*
$[P(CH_2C_6H_5)(C_6H_5)_3]$ $[HIr_4(CO)_{11}]$ in THF	2015 vs, 2005 vs, 1985 s, 1970 s, 1800 m	*b*
$[NMe_4]_2[Ir_6(CO)_{15}]$ in THF	2030 sh, 1970 s, 1910 sh, 1775 s, 1735 s	*c*
$Na_2[Ir_6(CO)_{15}]$ in THF	1993 s, 1984 s, 1928 w, 1788 m, 1735 m	*d*

[a] Vandenberg, D. M.; Choy, T. C.; Ford, P. C. *J. Organomet. Chem.* **1989**, *366*, 257. [b] Bau, R.; Chiang, M. Y.; Wei, C.-Y.; Garlaschelli, L.; Martinengo, S.; Koetzle, T. F. *Inorg. Chem.* **1984**, *23*, 4758. [c] Angoletta, M.; Malatesta, L.; Caglio, G. L. *J. Organomet. Chem.* **1975**, *94*, 99. [d] Maloney, S. D.; Kelley, M. J.; Koningsberger, D. C.; Gates, B. C. *J. Phys. Chem.* **1991**, *95*, 9406.

solid) includes ν_{CO} bands at 2082 s and 1984 s cm^{-1} (Figure 1A), indicating the presence of an iridium dicarbonyl species. This sample was treated in flowing CO at 1 bar. After about 8 h at 348 K, the two ν_{CO} bands changed to a new spectrum (2072 w, 2044 sh, 2035 s, 2011 m, 2000 sh, and 1765 mw cm^{-1}) (Figure 1B). This spectrum is similar to that of $[HIr_4(CO)_{11}]^-$ supported on MgO[7,21] (Table 2), which has been characterized by infrared and EXAFS spectroscopies and by extraction into solution with [PPN][Cl] in THF solution. The spectra of the supported tetrairidium cluster anions in zeolites and on MgO[7,21] resemble that of $[NBu_4][HIr_4(CO)_{11}]$[16] and that of $[P(CH_2C_6H_5)_3][HIr_4(CO)_{11}]$[19] in THF solution (Table 2), except that the peaks are broadened and the major terminal band is shifted about 20 cm^{-1} to higher wavenumbers and the bridging band shifted

about 60 cm^{-1} to lower wavenumbers, consistent with well-known ion-pairing effects.[21,28]

The wafer sample was removed from the cell in the drybox; it was light yellow, the color of $[NBu_4][HIr_4(CO)_{11}]$ in THF solution. Attempts were made to extract the iridium carbonyl species from the zeolite to allow a comparison of the infrared spectrum with that of $[NBu_4][HIr_4(CO)_{11}]$ in THF solution. The extractions were attempted under N_2 in the drybox with THF and with a solution of excess bis(triphenylphosphine)iminium chloride, [PPN][Cl], in THF. The wafer remained light yellow after the extraction attempt, while the solution remained colorless. No iridium carbonyls were observed in the solution by infrared spectroscopy, indicating that no such species were extracted from the zeolite.

In another experiment, a new wafer of the zeolite-supported $[Ir(CO)_2(acac)]$ sample was prepared and loaded into the infrared cell. The sample was treated in flowing CO at 348 K for 8 h to form the anion $[HIr_4(CO)_{11}]^-$, as described above. The temperature was then increased to 423 K. The infrared spectrum changed, and after 2 h a new spectrum (Figure 1C) having ν_{CO} bands at 2001 s, 1993 s, and 1710 m cm^{-1} was observed. The new spectrum resembles that of $[Ir_6(CO)_{15}]^{2-}$ supported on MgO, which has been characterized by infrared and EXAFS spectroscopies and by extraction into solution with [PPN][Cl] in THF.[21,29] The infrared spectra of these supported species resemble that of $[NMe_4]_2[Ir_6(CO)_{15}]$[16] and that of $[NMe_3CH_2Ph]_2[Ir_6(CO)_{15}]$[17] in THF (Table 2), except that the peaks are broadened and the frequency of the major terminal CO band of the encaged cluster is shifted about 12 cm^{-1} to higher frequency and that of the bridging ligand is shifted about 60 cm^{-1} to lower frequency relative to those of the cluster in solution. Again, the comparison indicates ion-pairing effects.[21]

The wafer unloaded in the drybox was light reddish brown. Again, extraction of the surface species from the zeolite was attempted with [PPN][Cl] in THF. The wafer remained reddish brown after the extraction attempt, while the solvent remained colorless. Moreover, no iridium carbonyls were detected in the extract solution with infrared spectroscopy, which indicates that no iridium carbonyls were extracted from the zeolite.

Reactivity of NaX Zeolite-Supported Iridium Carbonyl Clusters in the Presence of O_2. A new wafer sample, which was originally prepared from $[Ir(CO)_2(acac)]$ in NaX zeolite, was treated in flowing CO, first at 348 K for 4 h and then at 408 K for 2 h. After this treatment, the sample had an infrared spectrum (Figure 2A) similar to that of $[Ir_6(CO)_{15}]^{2-}$. The CO flow was then replaced by He containing 2% O_2. The infrared spectrum immediately changed; the band at 2000 cm^{-1} became sharper, and a new band at 2080 cm^{-1} appeared and increased in intensity (Figure 2B). After about 10 min, two intense bands in the ν_{CO} region (Figure 2C) were observed. When this oxidized sample was treated with flowing CO at 408 K, the band at 2080 cm^{-1} decreased in intensity (Figure 2D). After about 40 min in CO at 408 K, the spectrum of $[Ir_6(CO)_{15}]^{2-}$ reappeared (Figure 2E). The process was repeated three times with no substantial change in the resulting infrared spectra of the iridium carbonyls.

Decarbonylation of $[HIr_4(CO)_{11}]^-$ in NaX Zeolite: Infrared Spectroscopy. The zeolite incorporating the clusters with an infrared spectrum suggestive of $[HIr_4(CO)_{11}]^-$ was treated in flowing H_2 at 1 bar and 348 K for 30 min. The infrared spectrum was unchanged from that of Figure 1B; however, as the temperature increased beyond 398 K, the bands broadened, decreased in intensity, and shifted to lower frequencies. After the sample had been held for 2 h at 573 K in H_2, the ν_{CO} bands disappeared, indicating that the sample had been decarbonylated.

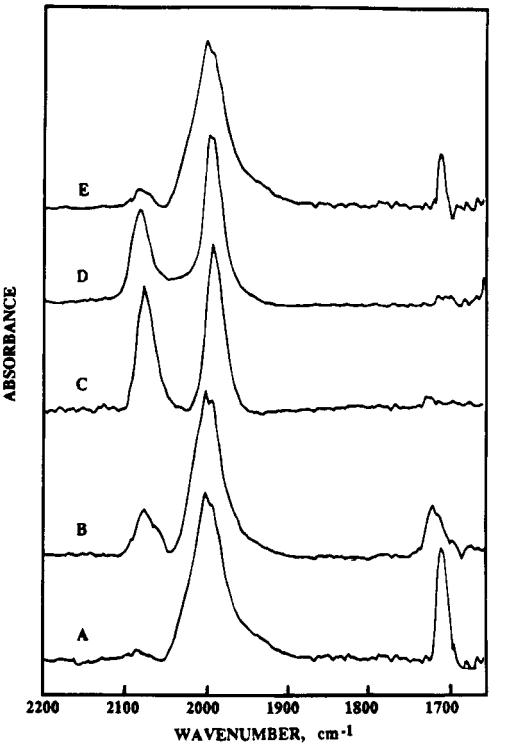

Figure 2. Infrared spectra characterizing the reactivity of NaX zeolite-supported clusters suggested to be $[Ir_6(CO)_{15}]^{2-}$ in O_2 at 408 K: (A) NaX zeolite-supported $[Ir_6(CO)_{15}]^{2-}$; (B) after treatment in flowing He/O_2 at 408 K for 2 min; (C) subsequent treatment in He/O_2 at 408 K for 10 min; (D) after CO treatment of sample C at 408 K for 15 min; (E) subsequent treatment in CO at 408 K for 40 min.

The decarbonylated sample was evacuated at 573 K for 30 min and cooled under vacuum to 298 K; it was beige.

EXAFS Results Characterizing Decarbonylated Clusters. The decarbonylated cluster was characterized by EXAFS spectroscopy. The normalized EXAFS function for each sample was obtained from the average of the X-ray absorption spectra by a cubic spline background subtraction. The EXAFS function was normalized to the height of the absorption edge. The raw EXAFS data (Figure 3A) show oscillations up to a value of k, the wave vector, of about 14 $Å^{-1}$, indicating the presence of near-neighbor high-Z backscatterers, which are inferred to be iridium.

The EXAFS analysis was done with the experimentally determined reference files referred to above. The raw EXAFS data were Fourier transformed with a k^2 weighting and no correction over the useful range ($3.68 < k < 14.59$ $Å^{-1}$). The major contributions were isolated by inverse Fourier transformation in the range $0.79 < r < 3.52$ Å (where r is the distance from the absorber Ir atom) to isolate the major contributions from low-frequency noise and higher-shell contributions. With the Koningsberger difference file technique,[29,30] the Ir−Ir contribution, the largest in the EXAFS spectrum, was estimated by calculating an EXAFS spectrum that agreed as closely as possible with the experimental results in the high-k range ($7.50 < k < 14.0$ $Å^{-1}$); the metal−support contributions in this region are small because the backscatterers in the support have low atomic weights. An EXAFS function calculated with the first-guess parameters was then subtracted from the data, with the residual spectrum being expected to represent the $Ir-O_{support}$ interactions. The difference file was estimated with two Ir−O contributions, as both short[31,32] and long[33,34] metal−support oxygen distances have been observed. As a first approximation, only four free parameters were estimated ($\Delta\sigma^2$, the Debye−

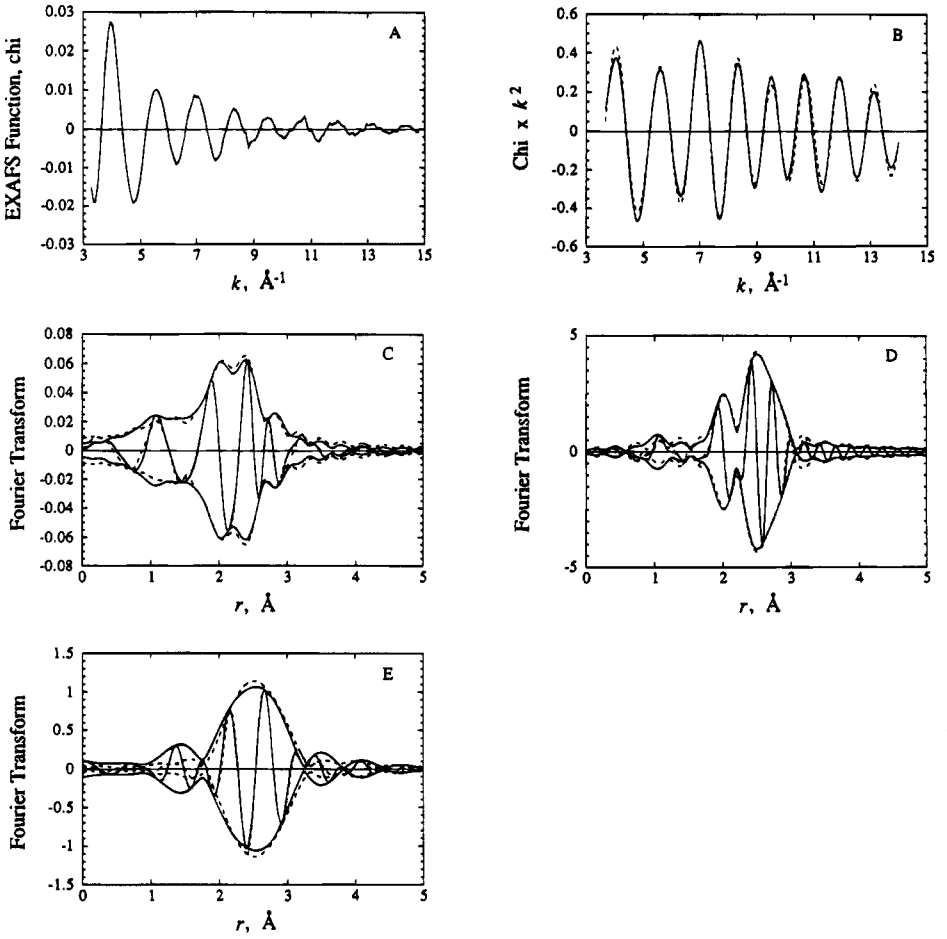

Figure 3. Results of EXAFS analysis obtained with the best calculated coordination parameters characterizing zeolite-supported Ir clusters prepared by decarbonylation of the Ir carbonyl clusters in NaX zeolite at 573 K in H_2: (A) raw EXAFS data; (B) experimental EXAFS (solid line) and sum of the calculated Ir−Ir + Ir−C + Ir−$O_{support}$ contributions (dashed line); (C) imaginary part and magnitude of Fourier transform (k^1-weighted, Δk = 3.66−13.80 Å^{-1}) of experimental EXAFS (solid line) and sum of the calculated Ir−Ir + Ir−C + Ir−$O_{support}$ contributions (dashed line); (D) imaginary part and magnitude of Fourier transform (k^3-weighted, Δk = 3.66−13.80 Å^{-1}) of experimental EXAFS (solid line) and sum of the calculated Ir−Ir + Ir−C + Ir−$O_{support}$ contributions (dashed line); (E) residual spectrum illustrating the EXAFS contributions characterizing the metal−support interaction: imaginary part and magnitude of Fourier transform (k^3-weighted, Δk = 3.66−10.00 Å^{-1}) of raw data minus calculated Ir−Ir + Ir−C EXAFS (solid line) and calculated Ir−O_l + Ir−O_s EXAFS (dashed line).

Waller factor, and ΔE_0, the inner potential correction, were set equal to 0) to shorten the computational time.

The first-guess Ir−Ir and Ir−$O_{support}$ contributions were then added and compared with the raw data in r space, and the fit was not yet satisfactory. Then the Ir−Ir contribution was subtracted from the data, and more accurate parameters for the contributions of the metal−support interface were determined by fitting the metal−support contributions to the residual spectrum with all eight parameters; the initial guesses for parameter estimation were determined by adjusting the coordination parameters to give the best agreement with the residual spectrum, both in k space and in r space. Even after many iterations, the fit was not good in the low-r region. It was inferred that another small contribution, attributed to a low-Z backscatterer, had to be accounted for. A difference file was calculated by subtracting the best estimated Ir−Ir + Ir−$O_{support}$ contribution from the experimental EXAFS function. The additional contribution was calculated by fitting the difference file with four adjustable parameters. The additional low-Z scatterer is not identified; it may be carbon remaining from the carbonyl ligands, and we tentatively refer to the contribution as Ir−C.

The Ir−Ir, Ir−C, and two Ir−$O_{support}$ contributions were then added, representing the overall fit of the data. To show the goodness of the fit for both the high-Z (Ir) and low-Z (O, C) contributions, the raw data are compared with the fit, both in k space (with k^2 weighting) and in r space (with both k^1 and k^3 weighting; Figure 3B−D). The agreement is good. The Ir−$O_{support}$ contributions are shown in the difference file of Figure 3E. The structure parameters are summarized in Table 3.

TABLE 3: EXAFS Results Characterizing the Iridium Clusters Formed by Decarbonylation of $[HIr_4(CO)_{11}]^-$ in NaX Zeolite[a,b]

shell	N	R, Å	$\Delta\sigma^2$, Å^2	ΔE_0, eV	EXAFS reference
Ir−Ir	3.0	2.71	0.0029	2.77	Pt−Pt
Ir−$O_{support}$					
Ir−O_l	2.2	2.71	0.0056	−8.14	Pt−O
Ir−O_s	0.85	2.20	0.0023	−7.32	Pt−O
Ir−C	0.72	1.83	0.0067	2.21	Ir−C

[a] Notation as in Table 1. [b] Estimated precision: N, ±20% (Ir−$O_{support}$, ±30%); R, ±2% (Ir−Ir, ±1%); $\Delta\sigma^2$, ±30%; ΔE_0, ±10%.

The number of parameters used to fit the data in this main-shell analysis is 16; the statistically justified number is approximately 20, estimated from the Nyquist theorem,[35] $n = (2\Delta k\Delta r/\pi) + 1$, where Δk and Δr, respectively, are the k and r ranges used in the forward and inverse Fourier transforms (Δk = 10.91 Å^{-1}; Δr = 2.73 Å).

Discussion

Parallels between Iridium Carbonyl Chemistry in Solution, on Metal Oxide Surfaces, and in Zeolite Cages. In

solution, $[Ir_4(CO)_{12}]$ is synthesized by carbonylation of iridium salts[36,37] or by carbonylation of $[Ir(CO)_2(acac)]$.[22] In basic solutions, $[Ir_4(CO)_{12}]$ is reductively carbonylated with KOH in methanol under CO to give a series of iridium carbonyl anions with nuclearities of 4, 6, and 8;[16] the reaction initially gives $[HIr_4(CO)_{11}]^-$,[19] then $[Ir_8(CO)_{22}]^{2-}$,[18] and finally $[Ir_6(CO)_{15}]^{2-}$.[17,20] The latter is the most stable of these anionic species under the carbonylation conditions in basic solution. In acidic solution, $[Ir_6(CO)_{15}]^{2-}$ is converted into two isomers of $[Ir_6(CO)_{16}]$.[16,20,38]

Similarly, the chemistry of the formation of iridium carbonyl clusters on basic MgO surfaces parallels that in basic solution, as follows:[7,21,29] The same reaction pathways in reductive carbonylation to form anionic iridium carbonyl clusters occur; the reactions give $[HIr_4(CO)_{11}]^-$,[7,21] $[Ir_8(CO)_{22}]^{2-}$,[21,39] and $[Ir_6(CO)_{15}]^{2-}$,[21,29] respectively, as the surface basicity increases. However, when the reductive carbonylation of iridium carbonyl is carried out on the weakly basic γ-Al_2O_3 surface, the formation of $[Ir_4(CO)_{12}]$, not anions, is observed.[22]

The results reported here support the hypothesis that the chemistry of the formation of iridium carbonyl clusters in the cages of NaX zeolite is nearly the same as that in basic solution and on basic MgO surfaces. The hypothesis is that reductive carbonylation of $[Ir(CO)_2(acac)]$ in NaX zeolite initially gives $[HIr_4(CO)_{11}]^-$, and then $[Ir_6(CO)_{15}]^{2-}$. The reactions on MgO have been suggested to involve surface OH groups and to produce carbonates.[40] The evidence for the presence of these clusters in the zeolites includes the infrared spectra and their comparisons with the spectra of these clusters on MgO and in solution. Furthermore, the conclusion based on the EXAFS spectra that the decarbonylated clusters are predominantly Ir_4 is supportive of the hypothesis that the precursor from which it was prepared was a tetranuclear cluster.

$[Ir_8(CO)_{22}]^{2-}$, which is formed from further reductive carbonylation of $[HIr_4(CO)_{11}]^-$ in basic solution[18] or on MgO,[21,39] was not observed to form in the zeolite cages; it is inferred to be too large to fit in the zeolite cages, and this interpretation is consistent with the inference that $[HIr_4(CO)_{11}]^-$ and $[Ir_6(CO)_{15}]^{2-}$ were confined in the cages. The formation of anionic iridium carbonyl clusters in NaX zeolite is not surprising because NaX zeolite is a relatively strong base.

Consistent with the pattern of chemistry stated above, whereby neutral iridium carbonyl clusters are formed in acidic solutions and on γ-Al_2O_3 surfaces, it has also been shown that the cages of NaY zeolite (which has only a weakly basic character) are a medium for the synthesis of neutral iridium carbonyl clusters, namely, $[Ir_4(CO)_{12}]$[11,12] and two isomers of $[Ir_6(CO)_{16}]$.[13,14] These results give an indication of the possibilities for modification of the reactivity in the solventlike cages of the zeolites by changing the Si to Al ratio.

In summary, there is a parallel between the chemistry of the formation of iridium carbonyl clusters in solution, on metal oxide surfaces, and in zeolite cages.

Ion Pairing of Iridium Carbonyl Clusters with NaX Zeolite Framework. The nature of the interactions between neutral metal carbonyls and Lewis acids, both in solution[41] and on surfaces,[42] has also been investigated. Ion pairing between anionic metal carbonyls and alkali metal ions in solution[43] or on surfaces[21] has been the subject of investigations for years. Generally, interaction of a metal carbonyl with a Lewis acid or with an alkali-metal ion via the oxygen of a carbonyl group results in a large decrease of the infrared absorption frequency of the carbonyl group, with the stretching frequencies of the noninteracting carbonyl ligands all shifting to slightly higher frequencies.

A comparison of the spectrum of $[HIr_4(CO)_{11}]^-$ in NaX zeolite (Figure 1B) with that of $[PPN][HIr_4(CO)_{11}]$ in THF (Table 2) shows a shift of the major terminal carbonyl band of the encaged species of about 15 cm^{-1} to higher frequency and a shift of the bridging carbonyl band of about 55 cm^{-1} to lower frequency. These shifts are consistent with ion pairing of $[HIr_4(CO)_{11}]^-$ with the Na^+ ions in the "solvating" zeolite cage, similar to the ion pairing of $[HIr_4(CO)_{11}]^-$ with the Mg cations on MgO surface[21] and that of $[HIr_4(CO)_{11}]^-$ with Na^+ in diethyl ether.[28] The relatively large shift of the bridging carbonyl band characteristic of NaX-supported $[HIr_4(CO)_{11}]^-$ suggests a strong interaction of the bridging carbonyl oxygen of the anion with Na^+ ions in the zeolite cage. Such an interaction is expected to result in a net electron withdrawal from the cluster, decreasing the back-bonding to the terminal carbonyl ligands, strengthening the carbon−oxygen bonds, and shifting the terminal carbonyl bands to higher frequencies.

Similar trends in the infrared band shifts have been observed for $[Ir_6(CO)_{15}]^{2-}$ in NaX zeolite (Figure 1C). A comparison with that of $[PPN]_2[Ir_6(CO)_{15}]$ in THF or that of $[NEt_4]_2[Ir_6(CO)_{15}]$ in THF (Table 2) shows a shift of the major terminal carbonyl band of the encaged species of about 12 cm^{-1} to higher frequency and a shift of the bridging carbonyl band of about 60 cm^{-1} to lower frequency. Again, these results suggest ion pairing of $[Ir_6(CO)_{15}]^{2-}$ with the Na^+ in the zeolite cage.

Reversible Oxidative Fragmentation and Reductive Carbonylation. Oxidative fragmentation of metal carbonyl clusters on the surfaces of amorphous metal oxides has been extensively investigated because (1) it could be used to synthesize nearly uniform, isolated surface-bound ensembles having the nuclearity of the cluster precursor,[44-46] and (2) there is a parallel between the oxidative fragmentation of supported metal carbonyl clusters and the disruption of small supported aggregates of metal resulting from exposure to CO.[44]

When the NaX-supported $[Ir_6(CO)_{15}]^{2-}$ was treated with oxygen, a reaction occurred to produce a species characterized by two sharp carbonyl bands (Figure 2B). A similar result has also been observed in the treatment of $[Ir_6(CO)_{16}]$ with oxygen;[14] the oxidized iridium carbonyl species was assigned as an $Ir^I(CO)_2$ complex on the basis of the comparison of its infrared spectrum with the spectrum of $[Ir(CO)_2(acac)]$[21] and that of $[Rh(CO)_2Cl]_2$.[47] Similarly, we infer that there was an oxidative fragmentation of $[Ir_6(CO)_{15}]^{2-}$ to form $Ir^I(CO)_2$ in the NaX zeolite.

The oxidized Ir carbonyl species in NaX was reductively carbonylated by treatment in CO to give back $[Ir_6(CO)_{15}]^{2-}$. This process was repeated three times; we infer that the oxidative fragmentation−reductive carbonylation cycle was reversible in the NaX zeolite cages, similar to that in NaY zeolite.[14]

Evidence of Entrapment of Iridium Carbonyl Clusters in NaX Zeolite Cages. One of the main issues complicating the synthesis and characterization of metal clusters in zeolites is the simultaneous formation of metal clusters or crystallites outside the zeolite crystallites, which is apparently often unavoidable. Much of the reported work with metal clusters and other nanostructures in zeolites has failed to include evidence to establish whether all the clusters were actually confined in the cages.

The results of the work summarized here are consistent with the inference that virtually all the iridium clusters were formed in and confined to the zeolite cages. The evidence is as follows:

(1) The synthesis conditions were chosen to remove iridium precursors and clusters from the outside of the zeolite crystals. The use of the neutral precursor $[Ir(CO)_2(acac)]$ has the

advantage of allowing removal of unconverted precursor that remained outside the crystallites by thorough washing with hexane; the infrared spectra indicate that the washing did not remove all the $[Ir(CO)_2(acac)]$ from the sample. Hence, we infer that the precursor remaining after the washing was inside the zeolite cages. Thus we infer that these precursors were the source of the iridium carbonyl clusters, which were entrapped in the zeolite cages.

(2) Because $[HIr_4(CO)_{11}]^-$ and $[Ir_6(CO)_{15}]^{2-}$ are soluble in THF, the lack of extraction of these anionic carbonyl clusters from NaX zeolite with [PPN][Cl] in THF indicates that the anions were entrapped in the zeolite cages, consistent with the fact that the clusters are too large to fit through the zeolite apertures. In contrast, the anionic iridium carbonyl clusters could be extracted from MgO that has pores large enough to allow the rapid diffusion of the clusters.

(3) The infrared spectra of NaX-supported $[HIr_4(CO)_{11}]^-$ and $[Ir_6(CO)_{15}]^{2-}$ gave evidence of ion pairing of the bridging CO ligands of the iridium carbonyl clusters with Na^+ ions, which are exchangeable ions located in the zeolite cages.

(4) Because $[Ir_8(CO)_{22}]^{2-}$ (which is a dimer with an Ir–Ir bond linking Ir_4 tetrahedra and has a length of about 15 Å, as determined by crystallographic data[18]) is formed in the reductive carbonylation of iridium carbonyls in basic solution and on the basic surface of MgO, the absence of its formation during the reductive carbonylation of $[HIr_4(CO)_{11}]^-$ in the relatively strongly basic NaX indicates that it is too large to fit in the zeolite supercage, which has a diameter of about 12 Å. The results give evidence that the zeolite-supported $[HIr_4(CO)_{11}]^-$, which has a diameter of about 9 Å (determined from the crystallographic data[19]) was entrapped in the zeolite cages and directly transformed in the cages into $[Ir_6(CO)_{15}]^{2-}$, which has a diameter of about 11 Å (determined from crystallographic data[17]).

(5) The reversibility of the cycles of oxidative fragmentation and reductive carbonylation of the iridium carbonyls might not be expected to occur if the iridium species were not in uniform environments such as those provided by the zeolite cages, which we infer help to stabilize the fragmented species and prevent their agglomeration to form particles of iridium metal. In contrast, $[Ir_4(CO)_{12}]$ formed on γ-Al_2O_3[22,48] and SiO_2,[48,49] for example, could not be reversibly fragmented and re-formed; instead, iridium particles formed.

In summary, the results are consistent with a ship-in-a-bottle synthesis. The precursor $[Ir(CO)_2(acac)]$ is inferred to be small enough to fit into the interior of the zeolite, as similar, but larger, metal carbonyls have been shown to fit: $[CpM(CO)_2]$, $[Cp^*M(CO)_2]$, and $[CpM(C_2H_4)_2]$ [M = Rh, Ir; Cp = C_5H_5; Cp* = $(CH^3)_5C_5$].[50] Furthermore, $[HIr_4(CO)_{11}]^-$ and $[Ir_6(CO)_{15}]^{2-}$ are small enough to fit in the supercages of NaX zeolite but too large to diffuse rapidly through the apertures (which have diameters of about 7.4 Å). Therefore, the clusters, once formed, were evidently trapped in the supercages.

Formation of Decarbonylated Ir_4 Clusters in NaX Zeolite. The decarbonylation of $[HIr_4(CO)_{11}]^-$ in NaX zeolite was carried out in flowing H_2 by gradually increasing the temperature. The terminal absorption bands shown by the infrared spectra decreased in intensity, broadened, and shifted to lower frequency as the temperature increased. The shift to lower frequency as the degree of decarbonylation increased suggests a strengthening of the interactions between the residual carbonyl bands and the iridium cluster as carbonyl ligands were removed. This result is similar to the results of Handy et al.,[51] who observed both the terminal and the bridging bands shifted to lower energy as the degree of decarbonylation of $[Pt_{15}(CO)_{30}]^{2-}$ on γ-Al_2O_3 increased. The decrease of CO coverage leads to the diminished dipole–dipole coupling between adjacent CO molecules and a smaller shift of the CO absorption bands.[52]

The iridium clusters prepared by decarbonylation of $[HIr_4(CO)_{11}]^-$ were characterized by EXAFS spectroscopy. The Ir–Ir coordination number of the cluster (Table 3) is 3.0, which is the same as the crystallographically determined Ir–Ir coordination number of $[HIr_4(CO)_{11}]^-$. Thus the structure of the cluster after decarbonylation is inferred to resemble the tetrahedral frame of $[HIr_4(CO)_{11}]^-$. The result indicates that there was negligible agglomeration or fragmentation of the clusters during decarbonylation, in agreement with the absence of higher shell Ir–Ir contributions.

In summary, these observations suggest that the structure of the iridium cluster frame after decarbonylation under mild conditions resembles that of the tetrahedra of $[HIr_4(CO)_{11}]^-$. The decarbonylated tetrairidium clusters are inferred to be similar to those that form by decarbonylation of $[HIr_4(CO)_{11}]^-$ supported on basic MgO;[7] it is possible that the clusters are stabilized by the rigid environment of the zeolite cages and migrate and sinter less rapidly than they would on a support with larger pores.

Conclusions

$[Ir(CO)_2(acac)]$ in the presence of CO in the supercages of NaX zeolite was converted by ship-in-a-bottle synthesis into iridium carbonyl clusters that are inferred to be $[HIr_4(CO)_{11}]^-$, which was converted into $[Ir_6(CO)_{15}]^{2-}$. The chemistry of the formation of these clusters in the zeolite parallels that in basic solutions and on basic MgO surfaces. The clusters interact by ion pairing with the zeolite framework. $[Ir_6(CO)_{15}]^{2-}$ in NaX zeolite cages was reversibly fragmented to iridium subcarbonyls. EXAFS spectra indicate that most of the clusters formed by decarbonylation of $[HIr_4(CO)_{11}]^-$ maintained the tetrahedral metal framework; the decarbonylated clusters are represented as Ir_4.

Acknowledgment. This work was supported by the National Science Foundation (CTS-9012910). The EXAFS data were analyzed with the Eindhoven University EXAFS Data Analysis Program, developed by M. Vaarkamp and D. C. Koningsberger. We also acknowledge the support of the U.S. Department of Energy, Division of Materials Sciences, under contract number DE-FG05-89ER45384, for its role in the operation and development of beam line X-11A at the National Synchrotron Light Source. The NSLS is supported by the Department of Energy, Division of Materials Sciences and Division of Chemical Sciences, under Contract No. DE-AC02-76CH00016. We are grateful to the staff of beam line X-11A for their assistance.

References and Notes

(1) Jacobs, P. A. In *Metal Clusters in Catalysis*; Gates, B. C., Guczi, L., Knözinger, H., Eds.; Elsevier: Amsterdam, 1986; p 357.
(2) Ozin, G. A.; Ozkar, S.; Moller, K.; Bein, T. *J. Am. Chem. Soc.* **1990**, *112*, 9575.
(3) Ozin, G. A.; Malek, A.; Prokopowicz, R.; Macdonald, P. M.; Ozkar, S.; Moller, K.; Bein, T. *Mater. Res. Soc. Symp. Proc.* **1991**, *233*, 109.
(4) Herron, N.; Wang, Y.; Eddy, M. M.; Stucky, G. D.; Cox, D. E.; Moller, K.; Bein, T. *J. Am. Chem. Soc.* **1989**, *111*, 530.
(5) Moller, K.; Eddy, M. M.; Stucky, G. D.; Herron, N.; Bein, T. *J. Am. Chem. Soc.* **1989**, *111*, 2564.
(6) Psaro, R.; Ugo, R. In *Metal Clusters in Catalysis*; Gates, B. C., Guczi, L., Knözinger, H., Eds.; Elsevier: Amsterdam, 1986; p 427.
(7) Maloney, S. D.; van Zon, F. B. M.; Koningsberger, D. C.; Gates, B. C. *Catal. Lett.* **1990**, *5*, 161.
(8) van Zon, F. B. M.; Maloney, S. D.; Gates, B. C.; Koningsberger, D. C. *J. Am. Chem. Soc.* **1993**, *115*, 10317.
(9) Chang, J.-R.; Koningsberger, D. C.; Gates, B. C. *J. Am. Chem. Soc.* **1992**, *114*, 6460.
(10) Lamb, H. H.; Wolfer, M.; Gates, B. C. *J. Chem. Soc., Chem. Commun.* **1990**, 1296.
(11) Kawi, S.; Gates, B. C. *Catal. Lett.* **1991**, *10*, 263.

(12) Kawi, S.; Chang, J.-R.; Gates, B. C. *J. Phys. Chem.* **1993**, *97*, 10599.
(13) Kawi, S.; Gates, B. C. *J. Chem. Soc., Chem. Commun.* **1991**, 994.
(14) Kawi, S.; Chang, J.-R.; Gates, B. C. *J. Am. Chem. Soc.* **1993**, *115*, 4830.
(15) Kawi, S.; Gates, B. C. *J. Chem. Soc., Chem. Commun.* **1992**, 702.
(16) Angoletta, M.; Malatesta, L.; Caglio, G. L. *J. Organomet. Chem.* **1975**, 94, 99.
(17) Demartin, F.; Manassero, M.; Sansoni, M.; Garlaschelli, L.; Martinengo, S. *J. Chem. Soc., Chem. Commun.* **1980**, 903.
(18) Demartin, F.; Manassero, M.; Sansoni, M.; Garlaschelli, L.; Raimondi, C.; Martinengo, S.; Canziani, F. *J. Chem. Soc., Chem. Commun.* **1981**, 528.
(19) Bau, R.; Chiang, M. Y.; Wei, C.-Y.; Garlaschelli, L.; Martinengo, S.; Koetzle, T. F. *Inorg. Chem.* **1984**, *23*, 4758.
(20) Stevens, R. E.; Lin, P. C. C.; Gladfelter, W. L. *J. Organomet. Chem.* **1985**, *287*, 133.
(21) Kawi, S.; Gates, B. C. *Inorg. Chem.*, **1992**, *31*, 2939.
(22) Kawi, S.; Chang, J.-R.; Gates, B. C. *J. Phys. Chem.* **1993**, *97*, 5375.
(23) Wyckoff, R. W. G. *Crystal Structures*, 2nd ed.; Wiley: New York, 1963; Vol. 1, p 10.
(24) Trömel, M.; Lupprich, E. *Z. Anorg. Chem.* **1975**, *414*, 160.
(25) Duivenvoorden, F. B. M.; Koningsberger, D. C.; Uh, Y. S.; Gates, B. C. *J. Am. Chem. Soc.* **1986**, *108*, 6254.
(26) Churchill, M. R.; Hutchinson, J. P. *Inorg. Chem.* **1978**, *17*, 3528.
(27) van Zon, J. B. A. D.; Koningsberger, D. C.; van't Blik, H. F. J.; Sayers, D. E. *J. Chem. Phys.* **1985**, *82*, 5742.
(28) Vandenberg, D. M.; Choy, T. C.; Ford, P. C. *J. Organomet. Chem.* **1989**, *366*, 257.
(29) Maloney, S. D.; Kelley, M. J.; Koningsberger, D. C.; Gates, B. C. *J. Phys. Chem.* **1991**, *95*, 9406.
(30) Kirlin, P. S.; van Zon, F. B. M.; Koningsberger, D. C.; Gates, B. C. *J. Phys. Chem.* **1990**, *94*, 8439.
(31) Emrich, R. J.; Mansour, A. N.; Sayers, D. E.; McMillan, S. T.; Katzer, J. R. *J. Phys. Chem.* **1985**, *89*, 4261.
(32) Lytle, F. W.; Greegor, R. B.; Marques, E. C.; Via, G. H.; Sinfelt, J. H. *J. Catal.* **1985**, *95*, 546.
(33) Koningsberger, D. C.; van Zon, J. B. A. D.; van't Blik, H. F. J.; Visser, G. J.; Prins, R.; Mansour, A. N.; Sayers, D. E.; Short, D. R.; Katzer, J. R. *J. Phys. Chem.* **1985**, *89*, 4075.
(34) Koningsberger, D. C.; Martens, J. H. A.; Prins, R.; Short, D. R.; Sayers, D. E. *J. Phys. Chem.* **1986**, *90*, 3047.
(35) Koningsberger, D. C.; Prins, R. *X-ray Absorption: Principles, Applications, Techniques of EXAFS, SEXAFS, and XANES*; Wiley: New York, 1988; p 395.
(36) Malatesta, L.; Caglio, G.; Angoletta, M. *Inorg. Synth.* **1972**, *13*, 95.
(37) Della Pergola, R.; Garlaschelli, L.; Martinengo, S. *J. Organomet. Chem.* **1987**, *331*, 271.
(38) Garlaschelli, L.; Martinengo, S.; Bellon, P. L.; Demartin, F.; Manassero, M.; Chiang, M. Y.; Wei, C.-Y.; Bau, R. *J. Am. Chem. Soc.* **1984**, *106*, 6664.
(39) Maloney, S. D.; Kelley, M. J.; Gates, B. C. *J. Organomet. Chem.* **1992**, *435*, 377.
(40) Xiao, F.-S.; Xu, Z.; Alexeev, O.; Gates, B. C. *J. Phys. Chem.* **1995**, *99*, 1548.
(41) Horwitz, C. P.; Shriver, D. F. *Advan. Organomet. Chem.* **1984**, *23*, 219.
(42) Tessier-Youngs, C.; Correa, F.; Ploch, D.; Burwell, R. J., Jr.; Shriver, D. F. *Organometallics* **1983**, *2*, 898.
(43) Darensbourg, M. Y. *Prog. Inorg. Chem.* **1985**, *33*, 221.
(44) Lamb, H. H.; Gates, B. C.; Knözinger, H. *Angew. Chem., Int. Ed. Engl.* **1988**, *27*, 1127.
(45) Gates, B. C. In *Catalyst Design: Progress and Perspectives*; Hegedus, L. L., Ed.; Wiley: New York, 1987; p 71.
(46) Gates, B. C.; Lamb, H. H. *J. Mol. Catal.* **1989**, *52*, 1.
(47) Smith, A. K.; Hugues, F.; Theolier, A.; Basset, J. M.; Ugo, R.; Zanderighi, G. M.; Bilhou, J. L.; Bilhou-Bougnol, V.; Graydon, W. F. *Inorg. Chem.* **1979**, *18*, 3104.
(48) Tanaka, K.; Watters, K. L.; Howe, R. F. *J. Catal.* **1982**, *75*, 23.
(49) Psaro, R.; Dossi, C.; Fusi, A.; Della Pergola, R.; Garlaschelli, L.; Roberto, D.; Sordelli, L.; Ugo, R.; Zanoni, R. *J. Chem. Soc., Faraday Trans.* **1992**, *88*, 369.
(50) Ozin, G. A.; Haddleton, D. M.; Gil, C. J. *J. Phys. Chem.* **1989**, *93*, 6710.
(51) Handy, B. E.; Dumesic, J. A.; Langer, S. H. *J. Catal.* **1990**, *88*, 369.
(52) Primet, M. *J. Catal.* **1984**, *88*, 273.

JP950172W